Different Microstructures of β-$NaYF_4$ Fabricated by Hydrothermal Process: Effects of pH Values and Fluoride Sources

Chunxia Li, Jun Yang, Zewei Quan, Piaoping Yang, Deyan Kong, and Jun Lin*

State Key Laboratory of Application of Rare Earth Resources, Changchun Institute of Applied Chemistry, Chinese Academy of Sciences, Changchun 130022, P. R. China, and Graduate University of the Chinese Academy of Sciences, Beijing 100049, P. R. China

Received June 21, 2007

β-$NaYF_4$ microcrystals with a variety of morphologies, such as microrod, hexagonal microprism, and octadecahedron, have been synthesized via a facile hydrothermal route. X-ray diffraction (XRD), scanning electron microscopy (SEM), transmission electron microscopy (TEM), high-resolution transmission electron microscopy (HRTEM), and photoluminescence (PL) spectra were used to characterize the samples. The intrinsic structural feature of β-$NaYF_4$ seeds and two important external factors, namely, the pH values in the initial reaction solution and fluoride sources, are responsible for shape determination of β-$NaYF_4$ microcrystals. It is found that the organic additive trisodium citrate (Cit^{3-}) as a shape modifier has the dynamic effect by adjusting the growth rate of different facets under different experimental conditions, resulting in the formation of the anisotropic geometries of various β-$NaYF_4$ microcrystals. The possible formation mechanisms for products with various architectures have been presented. A systematic study on the photoluminescence of Tb^{3+}-doped β-$NaYF_4$ samples with rod, prism, and octadecahedral shapes has shown that the optical properties of these phosphors are strongly dependent on their morphologies and sizes. This synthetic methodology appears to be general and promises to provide a gateway into other rare earth fluoride compounds.

1. Introduction

Anisotropy is an elementary property of single crystals, and the various facets or directions in a crystal may exhibit different physical and chemical properties. Recently, shape control of anisotropic nano- and microcrystals has aroused considerable attention due to the great potential for fundamental effects of morphology, dimensionality, and size on their physical, chemical, magnetic, and catalytic properties as well as for their application in optoelectronic devices.[1,2] A variety of methods are used for fabricating these anisotropic inorganic materials, most of which are synthesized in the presence of either hard templates or soft directing agents, including surfactants or polymers with complex functionalization patterns, which can direct the growth of inorganic crystals with controlled morphologies and architectures.[3] For instance, Yada and co-workers[4] described the synthesis of rare earth oxide nanotubes templated by dodecylsulfate assemblies. Carbon nanotubes could be used as sacrificial templates to generate nanorods of III−V compounds.[5] However, the addition of a template to the reaction system involves a complicated process and may result in impurity in the products. One can overcome these difficulties by developing the simple, one-step, and effective solution-phase methods for fabricating novel assemblies of the inorganic materials under template-free conditions or without the aid of other techniques. Because of its easily controllable reaction conditions and the relatively abundant reactant sources, the so-called soft chemical route, based on a solution process, might provide an attractive option for large-scale production of nano- and micromaterials with special morphologies.[6] Especially, hydrothermal treatment as a typical solution approach has been proved to be effective and convenient in preparing various inorganic materials with diverse controllable morphologies and architectures.[7] During the growth process of crystals, not only its intrinsic structures but also a series of external factors, such as reaction temperature, time, precursor solution pH value, and organic additives drastically influence the crystallization process and shape evolution of particles in a solution-based system.[8] Additionally, it has been demonstrated that the addition of simple salts can influence significantly the morphology of the

* Author to whom correspondence should be addressed. E-mail: jlin@ciac.jl.cn.

(1) Im, S. H.; Lee, Y. T.; Wiely, B.; Xia, Y. N. *Angew. Chem., Int. Ed.* **2005**, *44*, 2154.
(2) Cheng, F. C.; Zhao, J. Z.; Li, C. S.; Ma, H.; Chen, J.; Shen, P. W. *Inorg. Chem.* **2006**, *45*, 2038.
(3) (a) Li, F.; Ding, Y.; Gao, P. X.; Xin, X. Q.; Wang, Z. L. *Angew. Chem.* **2004**, *116*, 5350. (b) Li, M.; Lebeau, B.; Mann, S. *Adv. Mater.* **2003**, *15*, 2032. (c) Xia, Y. N.; Yang, P. D.; Sun, Y. G.; Wu, Y. Y.; Mayers, B.; Gates, B.; Yin, Y. D.; Kim, F.; Yan, H. Q. *Adv. Mater.* **2003**, *15*, 353.
(4) Yada, M.; Mihara, M.; Mouri, S.; Kuroki, M.; Kijima, T. *Adv. Mater.* **2002**, *14*, 309.
(5) Han, W.; Fan, S.; Li, Q.; Hu, Y. *Science* **1997**, *277*, 1287.
(6) (a) Wang, Z.; Qian, X. F.; Yin, J.; Zhu, Z. K. *Langmuir* **2004**, *20*, 3441. (b) Lu, C. H.; Qi, L. M.; Yang, J. H.; Wang, X. Y.; Zhang, D. Y.; Xie, J. L.; Ma, J. M. *Adv. Mater.* **2005**, *17*, 2562. (c) Yang, J.; Lin, C. K.; Wang, Z. L.; Lin, J. *Inorg. Chem.* **2006**, *45*, 8973. (d) Yang, J.; Quan, Z. W.; Kong, D. Y.; Liu, X. M.; Lin, J. *Cryst. Growth Des.* **2007**, *7*, 730.
(7) Liang, J. H.; Peng, Q.; Wang, X.; Zheng, X.; Wang, R. J.; Qiu, X. P.; Nan, C. W.; Li, Y. D. *Inorg. Chem.* **2005**, *44*, 9405.
(8) (a) Matijević, E. *Acc. Chem. Res.* **1981**, *14*, 22. (b) Zhang, H.; Yang, D. R.; Li, D. S.; Ma, X. Y.; Li, S. Z.; Que, D. L. *Cryst. Growth Des.* **2005**, *5*, 547.

10.1021/cm071668g CCC: $37.00
Published on Web 09/01/2007

products. Xia and co-workers[9] reported the synthesis of MoO_3 nanobelts and prism-like particles with good crystallinity and high surface areas by using different inorganic salts, such as KNO_3, $Ca(NO_3)_2$, and $La(NO_3)_3$.

Rare earth compounds, such as hydroxides,[10] oxides,[11] phosphates,[12] fluorides,[13] and vanadates,[14] have been extensively studied because of their potential applications in high-performance magnets, luminescent devices, catalysts, and other functional materials based on the electronic, optical, and chemical characteristics arising from the 4f electrons. Among them, the rare earth fluoride compounds with general formula like $NaREF_4$ (RE = rare earth), especially $NaYF_4$, possessing a high refractive index and low phonon energy,[15] have attracted more and more attention because they are regarded as excellent host matrixes for down-conversion (DC) and up-conversion (UC) processes. The crystal structure of $NaREF_4$ exhibits two polymorphic forms, namely, cubic (α-) and hexagonal (β-) phases, depending on the synthesis conditions and methods. Yan's group[16] opened up the possibility of a general methodology for shape control of α- and β-$NaREF_4$ nanostructures via the thermolysis of metal trifluoroacetates in high-boiling solvents of oleic acid/oleylamine/1-octadecene. As a representative example, here we focus on the preparation and shape evolution of $NaYF_4$ microcrystals. In the previous researches, $NaYF_4$ inorganic luminescent materials doped with different lanthanide ions or ion pairs[17] have been fabricated by the hydrothermal method. However, little has been done on the systematic manipulation of morphologies and architectures of monodisperse and uniform $NaYF_4$ microcrystals via the simple hydrothermal process so far.[18] Inorganic microcrystals with novel morphologies are of special significance in understanding the growth behavior and potential technological applications in microelectronic devices.[19] Moreover, the influence on the morphologies of rare earth fluoride compounds by the addition of simple salts XF ($X = Na^+$, NH_4^+, K^+, and H^+) to reaction system has drawn little attention. To the best of our knowledge, only several literatures demonstrated the effect of fluorides sources on the morphologies of EuF_3 and CeF_3.[20] To date, there is no report concerning the systematic study of the effect of fluorides sources on the morphological growth process of $NaYF_4$ microcrystals.

Accordingly, in this work, NaF and NH_4F are used as fluoride sources to fabricate β-$NaYF_4$ microcrystals with various well-defined morphologies, including microrod, hexagonal microprisms, and octadecahedra, via a facile and mild hydrothermal process. One of the characteristics of the above reactions is that no seeds or templates are required to control the sizes and morphologies of the products. The experimental results demonstrate that the anisotropic unit cell structure of the nucleated β-$NaYF_4$ seeds is first an important factor for shape control. Additionally, the different fluoride sources and pH values in the reaction system are also critical external parameters for determining the architectural features of the β-$NaYF_4$ microcrystals. The photoluminescence properties of β-$NaYF_4$:Tb^{3+} microparticles with different shapes are investigated to explore the optical and crystal quality of the products. The possible formation mechanisms for the hydrothermally synthesized β-$NaYF_4$ microcrystals with various morphologies are presented.

2. Experimental Section

Preparation. The rare earth oxides Y_2O_3 (99.999%) and Tb_4O_7 (99.999%) were purchased from Shanghai Yuelong New Materials Co., Ltd., and other chemicals were purchased from Beijing Chemical Co. All chemicals are of analytical grade reagents and used directly without further purification. Rare earth chloride stock solutions of 0.2 M were prepared by dissolving the corresponding metal oxide in hydrochloric acid at elevated temperature. In a typical procedure, 10 mL of YCl_3 (0.2 M) was added into 20 mL of aqueous solution containing 2 mmol of trisodium citrate (labeled as Cit^{3-}) to form the metal$-Cit^{3-}$ complex (1:1 molar ratio for Cit^{3-}/Y^{3+}). After vigorous stirring for 30 min, 25 mmol of NH_4F was added into the above solution. The pH of the mixture was adjusted to about 3 by adding HCl (1 M). After additional agitation for 15 min, the as-obtained mixing solution was transferred into a Teflon bottle held in a stainless steel autoclave, which was sealed and maintained at 180 °C for 24 h (according to the Peng$-$Robinson equation,[21] the pressure produced within the autoclave is calculated

(9) Xia, T.; Li, Q.; Liu, X. D.; Meng, J.; Cao, X. Q. *J. Phys. Chem. B* **2006**, *110*, 2006.

(10) Xu, A. W.; Fang, Y. P.; You, L. P.; Liu, H. Q. *J. Am. Chem. Soc.* **2003**, *125*, 1494.

(11) (a) Zhang, J.; Liu, Z. G.; Lin, J.; Fang, J. Y. *Cryst. Growth Des.* **2005**, *5*, 1527. (b) Si, R.; Zhang, Y. W.; You, L. P.; Yan, C. H. *Angew. Chem., Int. Ed.* **2005**, *44*, 3256. (c) Cao, Y. C. *J. Am. Chem. Soc.* **2004**, *126*, 7456. (d) Yu, T.; Joo, J.; Park, Y. I.; Hyeon, T. *Angew. Chem., Int. Ed.* **2005**, *44*, 7411.

(12) (a) Yu, M.; Wang, H.; Lin, C. K.; Li, G. Z.; Lin, J. *Nanotechnology* **2006**, *17*, 3245. (b) Heer, S.; Lehmann, O.; Haase, M.; Güdel, H. U. *Angew. Chem., Int. Ed.* **2003**, *42*, 3179.

(13) (a) Zhang, Y. W.; Sun, X.; Si, R.; You, L. P.; Yan, C. H. *J. Am. Chem. Soc.* **2005**, *127*, 3260. (b) Burns, J. H. *Inorg. Chem.* **1965**, *6*, 881. (c) Boyer, J. C.; Vetrone, F.; Cuccia, L. A.; Capobianco, J. A. *J. Am. Chem. Soc.* **2006**, *128*, 7444. (d) Wang, L. Y.; Yan, R. X.; Hao, Z. Y.; Wang, L.; Zeng, J. H.; Bao, J.; Wang, X.; Peng, Q.; Li, Y. D. *Angew. Chem., Int. Ed.* **2005**, *44*, 6054. (e) Yi, G. S.; Chow, G. M. *Chem. Mater.* **2007**, *19*, 341. (f) Wang, L. Y.; Li, Y. D. *Chem. Mater.* **2007**, *19*, 727. (g) Schäfer, H.; Ptacek, P.; Kömpe, K.; Haase, M. *Chem. Mater.* **2007**, *19*, 1396. (h) Stouwdam, J. W.; van Veggel, F. C. J. M. *Langmuir* **2004**, *20*, 11763. (i) Sudarsan, V.; van Veggel, F. C. J. M.; Herring, R. A.; Raudsepp, M. *J. Mater. Chem.* **2005**, *15*, 1332. (j) Sivakumar, S.; van Veggel, F. C. J. M.; Raudsepp, M. *J. Am. Chem. Soc.* **2005**, *127*, 12464. (k) Sudarsan, V.; Sivakumar, S.; van Veggel, F. C. J. M.; Raudsepp, M. *Chem. Mater.* **2005**, *17*, 4736.

(14) (a) Huignard, A.; Buissette, V.; Laurent, G.; Gacoin, T.; Boilot, J. P. *Chem. Mater.* **2002**, *14*, 2264. (b) Jia, C. J.; Sun, L. D.; Luo, F.; Jiang, X. C.; Wei, L. H.; Yan, C. H. *Appl. Phys. Lett.* **2004**, *84*, 5305.

(15) Diamente, P. R.; Raudsepp, M.; van Veggel, F. C. J. M. *Adv. Funct. Mater.* **2007**, *17*, 363.

(16) Mai, H. X.; Zhang, Y. W.; Si, R.; Yan, Z. G.; Sun, L. D.; You, L. P.; Yan, C. H. *J. Am. Chem. Soc.* **2006**, *128*, 6426.

(17) (a) Zeng, J. H.; Su, J. S.; Li, Z. H.; Yan, R. X.; Li, Y. D. *Adv. Mater.* **2005**, *17*, 2119. (b) Zeng, J. H.; Li, Z. H.; Su, J.; Wang, L. Y.; Yan, R. X.; Li, Y. D. *Nanotechnology* **2006**, *17*, 3549. (c) Wang, X.; Zhuang, J.; Peng, J.; Li, Y. D. *Inorg. Chem.* **2006**, *45*, 6661. (d) Sun, Y. J.; Chen, Y.; Tian, L. J.; Yu, Y.; Kong, X. G.; Zhao, J. W.; Zhang, H. *Nanotechnology* **2007**, *18*, 275609. (e) Zhuang, J.; Liang, L.; Sung, H. H. Y.; Yang, X.; Wu, M.; Williams, Ian D.; Feng, S.; Su, Q. *Inorg. Chem.* **2007**, *46*, 5404.

(18) Wang, Z. J.; Tao, F.; Yao, L. Z.; Cai, W. L.; Li, X. G. *J. Cryst. Growth* **2006**, *290*, 296.

(19) Wang, Q. Q.; Xu, G.; Han, G. R. *Cryst. Growth Des.* **2006**, *6*, 1776.

(20) (a) Wang, M.; Huang, Q. L.; Hong, J. M.; Chen, X. T.; Xue, Z. L. *Cryst. Growth Des.* **2006**, *6*, 1972. (b) Wang, M.; Huang, Q. L.; Hong, J. M.; Chen, X. T.; Xue, Z. L. *Cryst. Growth Des.* **2006**, *6*, 2169. (c) Zhu, L.; Qin, L.; Liu, X. D.; Li, J. Y.; Zhang, Y. F.; Meng, J.; Cao, X. Q. *J. Phys. Chem. C* **2007**, *111*, 5898.

(21) (a) Rajamathi, M.; Seshadri, R. *Curr. Opin. Solid State Mater. Sci.* **2002**, *6*, 337. (b) Chen, Z. X.; Gu, F. Y.; Hu, W. M. *Chemistry Industry Thermodynamics*, 2nd ed.; Publishing Company of Chemistry Industry: Beijing, China, 2003.

Table 1. Summary of the Experiment Conditions and the Corresponding Morphologies and Dimensions of the Samples[a]

sample	molar ratio Cit^{3-}:Y^{3+}	fluoride source	pH	morphology	length (μm)	diameter (μm)
S1	1:1	NH_4F	3	prismatic microrod with shape ends	14	1.4
S2	2:1		3	prismatic microrod with shape ends	7.8	1.4
S3	4:1		3	prismatic microrod with shape ends	1.8	1.4
S4	1:1		7	prismatic microrod with conical ends	14	4
S5	1:1		10	hexagonal microprism with the hexagon concave centers	5	4.5
S6	1:1	NaF	3	irregularity	2	1
S7	1:1		11	octadecahedron	1 (edge)	
S8	1:1		10	hexagonal microprism with protruding centers	0.6	2.3

[a] All samples were hydrothermally treated at 180 °C for 24 h.

to be approximately 550 bar). As the autoclave was cooled to room temperature naturally, the precipitates were separated by centrifugation, washed with deionized water and ethanol in sequence, and then dried in air at 80 °C for 12 h. The as-prepared product was denoted as **S1**. Other samples (**S4**−**S8**) were prepared by the similar procedure, except for different fluoride sources and pH conditions. The pH of the mixture was adjusted to a specific value by adding NaOH solution (3 M), ammonia solution (25%), or HCl (1 M) solution. In addition, **S2** and **S3** were prepared with 2:1 and 4:1 molar ratio of Cit^{3-}/Y^{3+}, and other conditions are the same as those for synthesizing **S1**. The experimental conditions are summarized in Table 1. It should be stated that all samples were hydrothermally treated at 180 °C for 24 h.

Characterization. Power X-ray diffraction (XRD) measurements were performed on a Rigaku-Dmax 2500 diffractometer at a scanning rate of 15°/min in the 2θ range from 10° to 80°, with graphite-monochromatized Cu Kα radiation (λ = 0.154 05 nm). SEM micrographs were obtained using a field emission scanning electron microscope (FE-SEM, XL30, Philips). Low- to high-resolution transmission electron microscopy (TEM) was performed using a FEI Tecnai G2 S-Twin instrument with a field emission gun operating at 200 kV. Images were acquired digitally on a Gatan multiople CCD camera. The photoluminescence (PL) excitation and emission spectra were recorded with a Hitachi F-4500 spectrophotometer equipped with a 150 W xenon lamp as the excitation source. The PL lifetimes of the samples were measured with a Lecroy Wave Runner 6100 digital oscilloscope (1 GHz) using a tunable laser (pulse width = 4 ns) as the excitation source (Continuum Sunlite OPO). All the measurements were performed at room temperature.

3. Results and Discussion

Structures. The composition and phase purity of the products were first examined by XRD. XRD patterns of the samples prepared by using NH_4F as fluoride source and keeping the molar ratio of Cit^{3-}/Y^{3+} as 1:1 with hydrothermal treatment at 180 °C for 24 h under various pH conditions of (a) pH = 7, (b) pH = 3, and (c) pH = 10 are shown in Figure 1. The diffraction peaks of the three samples can be indexed as a pure hexagonal (β-) phase (space group $P6_3/m$), which coincides well with the literature values (JCPDS No. 16-0334). It is worth pointing out that the XRD patterns also indicate that there is a large difference from each other in the relative intensities based on (110), (100), (101), and (201) peaks for three samples, indicating the possibility of different preferential orientation growth under different pH conditions. Moreover, as can be seen from the XRD patterns, the high crystallinity can be obtained at a relatively low hydrothermal treatment temperature (180 °C). If NH_4F was replaced by NaF as fluoride source, the XRD patterns of as-prepared products at different pH values (3, 11, 10) are shown in Figure 2. As can be seen, all the peaks of each sample are characteristic of a pure β-phase of $NaYF_4$, but the relative intensities are different from those obtained using NH_4F as fluoride source.

Morphologies. The morphologies and dimensions of the products are summarized in Table 1. From Table 1 it is found that the fluoride sources and pH values of the initial reaction solutions have great effects on the morphologies and dimensions of the final products. The detailed effects of these conditions on the shapes of the final products are shown in the following paragraphs.

Using the same fluoride source, the different pH values of the initial reaction solution show a large impact on the crystal growth of $NaYF_4$, and thus they influence the morphologies and microstructures of products.

A. NH_4F as Fluoride Source. The SEM images provide direct information about the size and typical shapes of the as-synthesized $NaYF_4$ samples grown under different experimental conditions. Figure 3 illustrates the representative SEM images of β-$NaYF_4$ prepared using NH_4F as fluoride source at different pH values. The product (**S1**) obtained at pH = 3 is composed of a great deal of microrods with a uniform size of 14 μm in length and 1.4 μm in diameter (Figure 3A). This suggests the high yield and good uniformity achieved with this approach. The magnified SEM image (Figure 3B) shows clearly that the products are prismatic microrods with smooth and flat surfaces as well as sharp and cracked ends. More careful examination of a typical rod, shown in the inset of Figure 3B, indicates that these rods actually have solid interiors. Experimental studies with different contents of Cit^{3-} have also provided evidence to support this result. When all the other conditions remain unchanged, with the increase of Cit^{3-}:Y^{3+} molar ratios, up to 2:1 and 4:1, the morphology of the corresponding products is basically maintained, but the length reduces from 14 to 7.8 and 1.8 μm, respectively, as illustrated in Figure 4. It can be seen clearly that these microrods are of solid interiors. This also indicates that the capping ability of the Cit^{3-} increases significantly with the increase of its amount so that the crystal growth is remarkably restricted along the [0001] direction, leading to the smaller β-$NaYF_4$ microrods as observed. The observation based on the TEM image of a representative rod for **S1** further reveals the sharp ends of the crystal morphology (Figure 6A). As disclosed by the corresponding HRTEM image, the interplanar distance between the adjacent lattice fringes is determined as ~0.36 nm, as shown in Figure 6B. This plane can be well-indexed as the *d*-spacing value of the (0001) plane of the β-$NaYF_4$

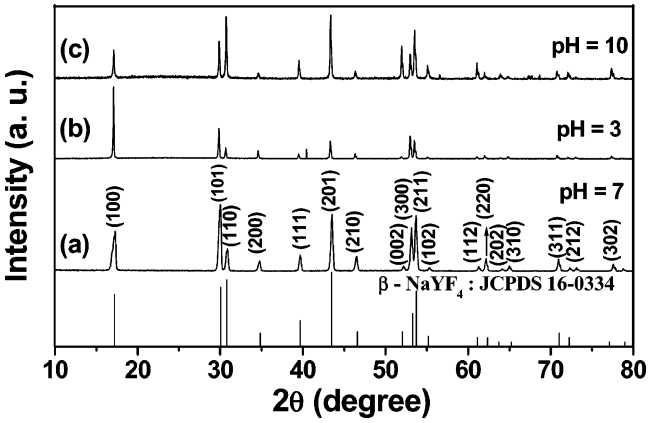

Figure 1. The XRD patterns of the as-prepared $NaYF_4$ products using NH_4F as fluoride source at different pH values after 24 h at 180 °C (1:1 molar ratio for Cit^{3-}/Y^{3+}) and the standard data of hexagonal β-$NaYF_4$ (JCPDS 16−0334) as a reference: (a) pH = 7, (b) pH = 3, (c) pH = 10.

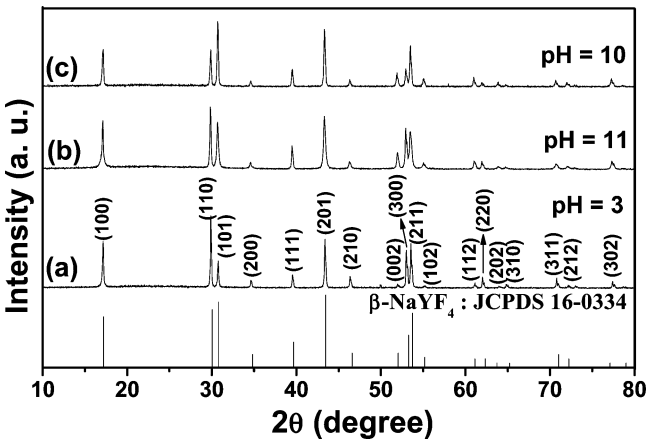

Figure 2. The XRD patterns of the as-prepared β-$NaYF_4$ products using NaF as fluoride source at different pH values after 24 h at 180 °C (1:1 molar ratio for Cit^{3-}/Y^{3+}) and the standard data of hexagonal β-$NaYF_4$ (JCPDS 16−0334) as a reference: (a) pH = 3, (b) pH = 11, (c) pH = 10.

crystal, confirming that the microrods show a preferred growth along the *c*-axis, namely the [0001] direction.[22] Hydrothermal treatment of an initial solution with pH = 7 also results in the formation of microrods on a large scale (Figure 3C). However, compared with **S1**, the hexagonal microrods have no obvious change in the mean length (about 14 μm), whereas the diameter of the particles increases remarkably from 1.4 to 4 μm. Furthermore, the ends of rods are of conical structure, as shown in Figure 3D. If the pH value of initial solution is increased to 10.0 with ammonia solution (25%), the morphology of the products varies greatly. It can be clearly seen from part E of Figure 3 that there are a large quantity of hexagonal microprisms over the entire surface of the substrates. Further investigation under higher magnification reveals prismatic structures with perfect uniformity, monodispersity, and well-defined crystallographic facets (Figure 3F). Interestingly, the surfaces of top/bottom have very regular hexagonal concave centers, as shown in the inset of Figure 3F. Analysis of a number of the microprisms shows that the average height and diameter of these microprisms are about 5 and 4.5 μm, respectively. TEM images can provide further insight into the micrometer-scale

(22) Liang, Y.; Zhang, X. T.; Qin, L.; Zhang, E.; Gao, H.; Zhang, Z. G. *J. Phys. Chem. B* **2006**, *110*, 21593.

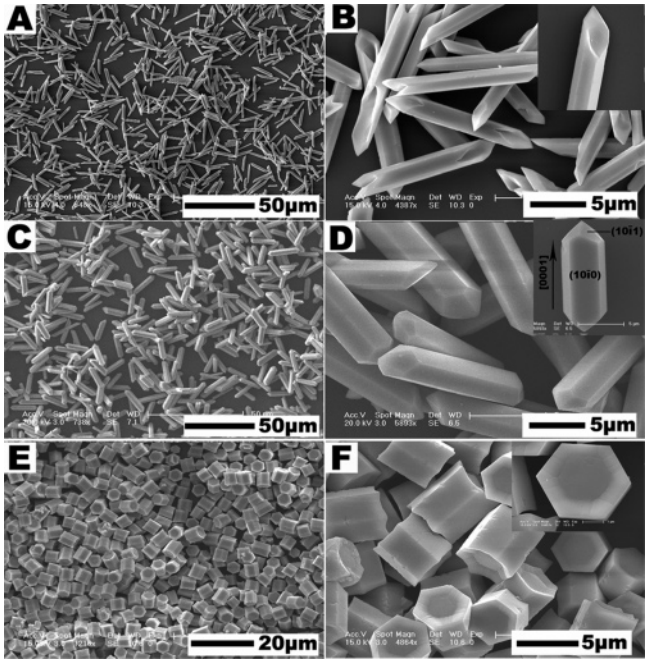

Figure 3. The influence of the pH values on the shapes of $NaYF_4$ microcrystals with NH_4F as fluoride source. (A, B) Prismatic microrods with cracked ends obtained at pH = 3. (C, D) Prismatic microrods with conical ends obtained at pH = 7. (E, F) Hexagonal microprisms obtained at pH = 10. These samples were hydrothermally treated at 180 °C for 24 h (1:1 molar ratio for Cit^{3-}/Y^{3+}).

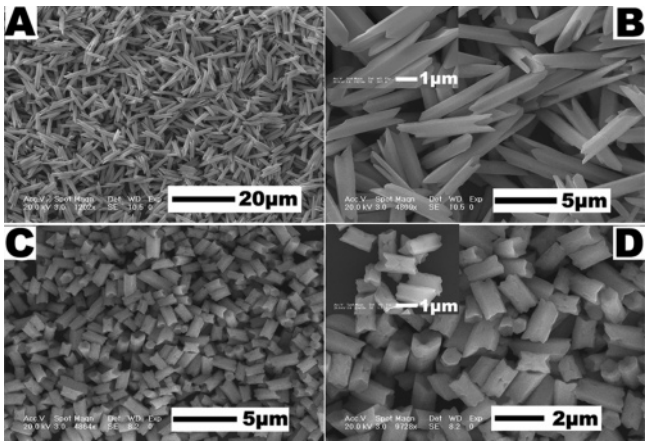

Figure 4. SEM images of β-$NaYF_4$ prismatic microrods prepared at pH = 3 with the different molar ratio of Cit^{3-}/Y^{3+}: 2:1 (A, B) and 4:1 (C, D).

details of the hexagonal prisms. The rectangular-like cross-section with scraggly top/bottom surfaces (Figure 6C) and regular hexagonal cross-section can be observed (Figure 6D), which correspond to individual hexagonal microprisms standing on the side face perpendicular to the substrate and lying flat on the bottom face parallel to the substrate, respectively. The edge length and diameter of the rectangle and hexagon are about 5 and 4.5 μm, respectively. These values are consistent with those observed from SEM images (Figure 3E, F).

B. NaF as Fluoride Source. When NaF replaces NH_4F as fluoride source and the other reaction conditions remain unchanged, the morphologies of the products are quite different from those observed using NH_4F as fluoride source, as shown in Figure 5. At pH = 3, the irregularly shaped β-$NaYF_4$ crystals are shown in parts A and B in Figure 5. The mean size is 2 μm in length and 1 μm in diameter,

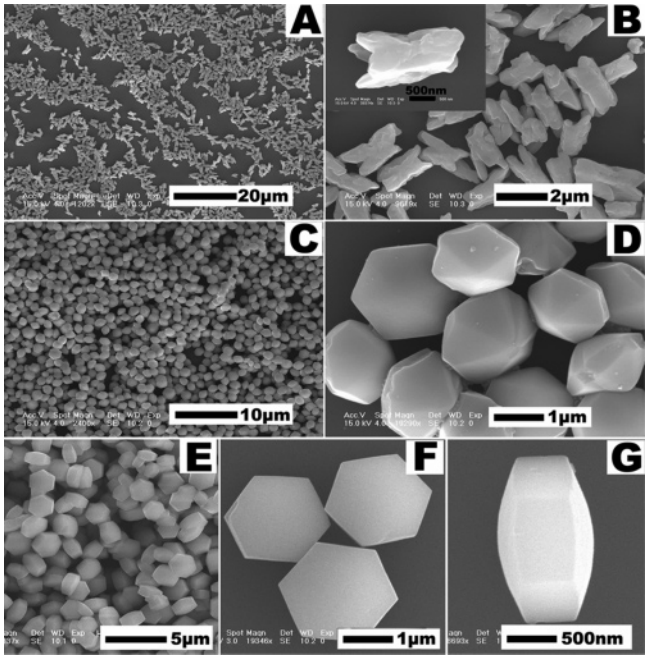

Figure 5. The influence of the pH values on the shapes of $NaYF_4$ microcrystals using NaF as fluoride source. (A, B) Irregular structure obtained at pH = 3. (C, D) Octadecahedral structure obtained at pH = 11 adjusted with 3 M NaOH. (E, F, G) Hexagonal prismatic structure obtained at pH = 10 adjusted with ammonia solution (25%). These samples were hydrothermally treated at 180 °C for 24 h (1:1 molar ratio for Cit^{3-}/Y^{3+}).

respectively. Moreover, the surfaces of the crystals are very coarse. Upon a further increase of the pH value up to 11 with the addition of NaOH, unique and regular octadecahedral β-$NaYF_4$ microcrystals are yielded in large quantities (Figure 5C). The average edge length of these octadecahedra is about 1 μm (Figure 5D). To the best of our knowledge, this is the first synthesis of β-$NaYF_4$ crystals with well-defined, regular, and uniform octadecahedral morphology. A corresponding TEM image of an octadecahedron is shown in Figure 6E. The contrast between the edge parts and the center part further reveals the octadecahedral structure. The spacing of the lattice fringes are found to be about 0.52 nm, as shown in Figure 6F. This plane can be attributed to the $(10\bar{1}0)$ plane of the β-$NaYF_4$ crystal.[23] However, if the solution pH is adjusted to 10 with ammonia solution (25%), the products are of hexagonal microprismatic structures (Figure 5E−G) with very smooth surfaces, whose mean diameter and height are 2.3 μm and 0.6 μm, respectively. Further careful examination reveals that the center part of hexagonal prisms is more protruding than that of the edge parts (Figure 5G).

Growth Mechanism. A series of controlled experiments demonstrates that the shape evolutions of β-$NaYF_4$ microcrystals are influenced by external factors such as the pH values in the initial solution and fluoride sources in conjunction with the intrinsic crystallographic structure of β-$NaYF_4$ crystals.

Intrinsic Structure: Crystalline Phase of Nucleating Seeds. One of the critical factors responsible for the shape determination of the nano- and microcrystals is the crystallographic phase of the initial seed. Once the crystalline phase

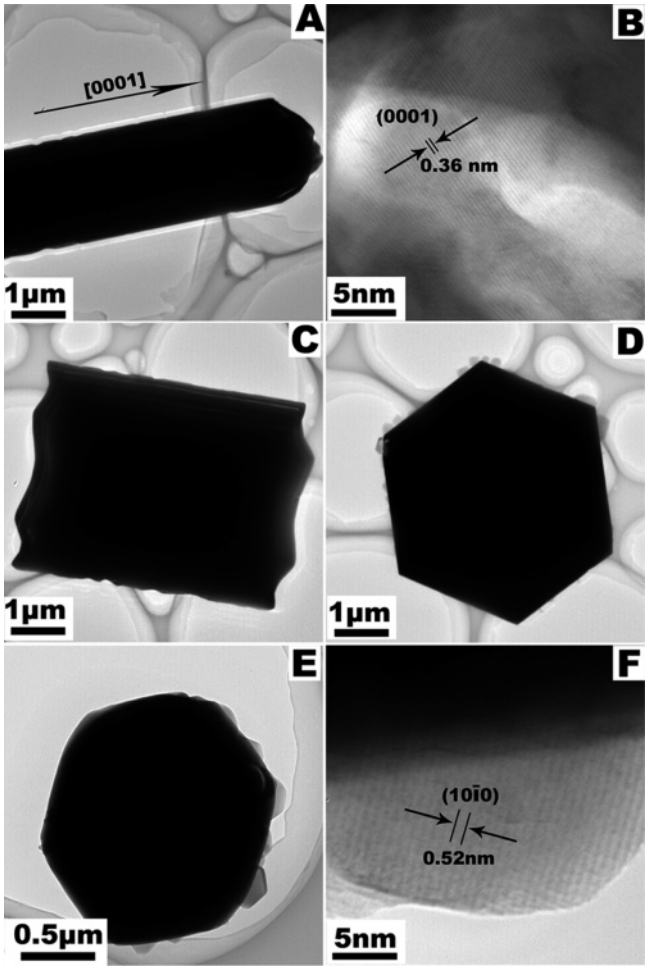

Figure 6. TEM and HRTEM images of the samples. (A, B) TEM and HRTEM images of microrod structure (**S1**). (C, D) TEM images of hexagonal microprismatic structure with hexagonal concave centers (**S5**). (E, F) TEM and HRTEM images of octadecahedral structure (**S7**).

is determined, the characteristic cell structures of the seeds strongly affect the further crystal growth.[24] In our experiments, it is noted that all samples experience an $\alpha \rightarrow \beta$ phase transformation process accompanied with morphology variations during the crystal growth. To shed light on the shape evolution of β-$NaYF_4$ crystals, taking **S1** as an example, detailed time-dependent experiments were carried out under similar reaction conditions for synthesizing **S1**. The XRD patterns and the corresponding SEM images of the intermediates obtained at different reaction time intervals are shown in Figures 7 and 8, respectively. They reveal that the intermediates display distinctively different XRD patterns and morphologies at different reaction periods. The hydrothermal treatment for 1 h leads to the formation of a pure cubic (α-) $NaYF_4$ phase (Figure 7a), which is in accord with the literature values (JCPDS 06-0342). A corresponding typical SEM image reveals that α-$NaYF_4$ products are composed of spherical nanoparticles with a mean diameter of 35 nm, as shown in Figure 8A. But in the present environment, α-phase $NaYF_4$ is unstable and is susceptible to slow phase transformation. A dissolution−renucleation process for nanospheres takes place, and the more stable

(23) Wang, L. Y.; Li, Y. D. *Nano Lett.* **2006**, *6*, 1645.

(24) Jun, Y.-w.; Lee, J.-H.; Choi, J.-s.; Cheon, J. *J. Phys. Chem. B* **2005**, *109*, 14795.

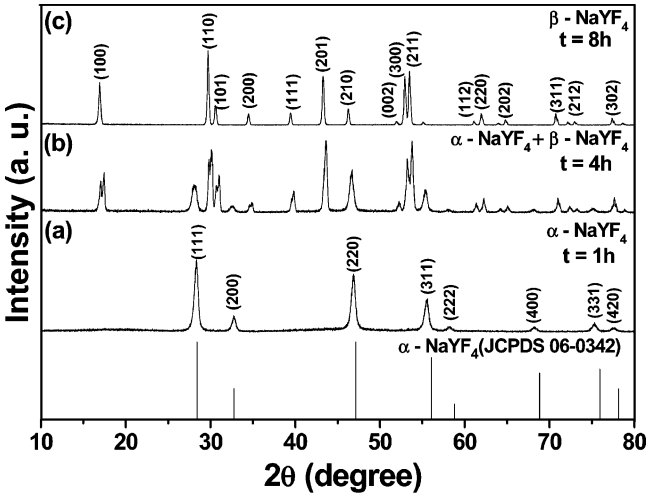

Figure 7. XRD patterns for $NaYF_4$ samples under similar conditions for synthesizing **S1** as a function of reaction time and the standard data of cubic α-$NaYF_4$ (JCPDS 06−0342) are given as a reference: (a) 1 h, (b) 4 h, (c) 8 h.

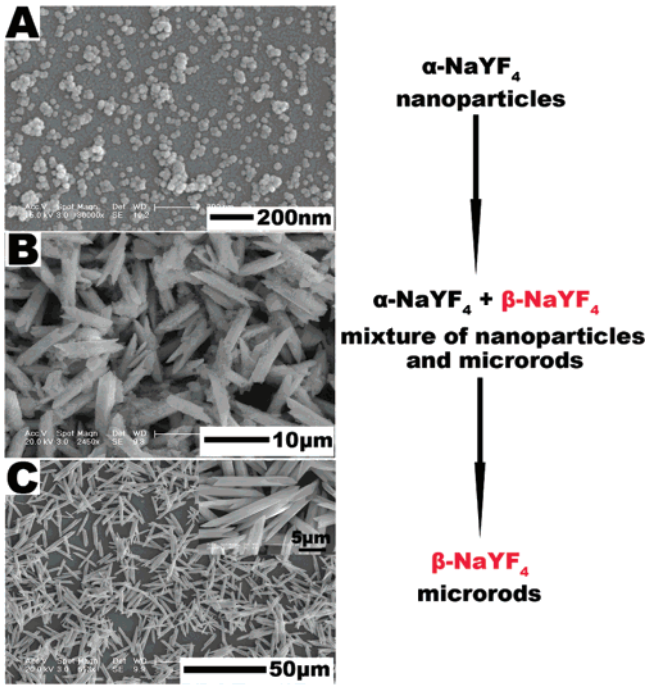

Figure 8. SEM images for $NaYF_4$ samples under similar conditions for synthesizing **S1** as a function of reaction time: (A) 1 h, (B) 4 h, (C) 8 h.

crystalline phase, namely β-$NaYF_4$ emerges with the reaction proceeding for 4 h (Figure 7b). This intermediate product consists of a mixture of hexagonal microrods 9.5 μm in length and some irregular particles on the surface of the hexagonal microrods, as presented in Figure 8B. At $t = 8$ h, the α-phase disappears completely and only the β-phase exists (Figure 7c). The corresponding shape of the product is fairly uniform hexagonal microrods with an average length of 14 μm (Figure 8C), similar to that of **S1** except for the difference in the sizes. On the basis of the above analyses, it can be concluded that the conversion from cubic to hexagonal phase directly results in the dramatic morphology changes of the products. This further confirms that the inherent crystal structure of seeds plays an important role in the formation of nano- and microstructures. The cubic α-$NaYF_4$ seeds have isotropic unit cell structures, which

Scheme 1. Schematic Diagram Showing the Anisotropy of the β-$NaYF_4$ Hexagonal Rod or Prismatic (a) and Octadecahedral (b) Structures

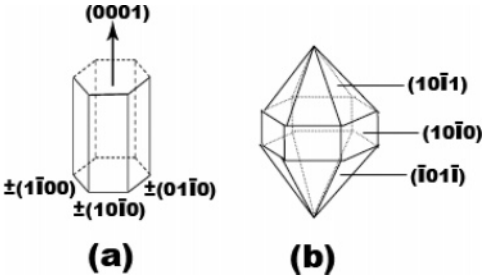

generally induce the isotropic growth of particles, and therefore, spherical particles are observed in order to minimize the surface energy of crystal facets. In contrast, β-$NaYF_4$ seeds have anisotropic unit cell structures, which can induce anisotropic growth along crystallographically reactive directions, resulting in the formation of hexagonal-shaped structures, as reported previously for the formation of hexagonal nanoplates of β-$NaYF_4$:Yb^{3+}/Er^{3+}.[25]

External Factors. The use of different fluoride sources and pH values in the initial reaction solution are the external key factors in determining the morphologies of the final products.

A. pH Values with NH_4F as Fluoride Source. When the other experimental conditions are the same, the exact mechanism for the morphology variations of $NaYF_4$ grown under different pH values using NH_4F as fluoride source might be explained in terms of the kinetically induced anisotropic growth mechanism put forward by Jun and co-workers.[26] As known, the organic molecules (Cit^{3-}) can form strong complexes with Y^{3+} ions through coordination interaction.[14a] This can be confirmed by the white precipitates produced after directly mixing the aqueous solution containing Y^{3+} and Cit^{3-}. In addition, Murphy[27] had claimed that the preferential adsorption of molecules and ions in solution onto different crystal facets directs the growth of particles into various shapes by controlling the growth rates along different crystal axes. Simultaneously, it is noteworthy that, for β-$NaYF_4$ crystals with hexagonal prism or rod shapes, the surfaces are typically {0001} for top/bottom planes and a family of six energetically equivalent {10$\bar{1}$0} prismatic side planes [(10$\bar{1}$0), ($\bar{1}$010), (0$\bar{1}$10), (01$\bar{1}$0), (1$\bar{1}$00), and ($\bar{1}$100)] on the basis of the known or similar models,[19,28] as shown in Scheme 1a. In the present situations, the differences in pH values show a significant effect on the selective adsorption of Cit^{3-} onto the different surfaces of growing $NaYF_4$ crystallites, giving rise to the difference of the growth rates between different crystallographic directions. At pH = 3, Cit^{3-} anions possibly bind strongly to {10$\bar{1}$0} surfaces of the growing β-$NaYF_4$ crystallites. So the particles grow

(25) Wei, Y.; Lu, F. Q.; Zhang, X. R.; Chen, D. P. *Chem. Mater.* **2006**, *18*, 5733.
(26) Jun, Y. W.; Choi, J. S.; Cheon, J. *Angew. Chem., Int. Ed.* **2006**, *45*, 3414.
(27) Murphy, C. J. *Science* **2002**, *298*, 2139.
(28) (a) Hsuch, T. J.; Chang, S. J.; Lin, Y. R.; Tsai, S. Y.; Chen, I. C.; Hsu, C. L. *Cryst. Growth Des.* **2006**, *6*, 1282. (b) Laudise, R. A.; Ballman, A. A. *J. Phys. Chem.* **1960**, *64*, 688. (c) Laudise, R. A.; Kolb, E. D.; Caporaso, A. J. *J. Am. Chem. Soc.* **1964**, *47*, 9.

preferentially along the [0001] direction and the growth rate along the [10$\bar{1}$0] direction is much slower than that along the [0001] direction, leading to the formation of 1D prismatic microrods with an average length up to 14 μm. This is coincident with the XRD results. In the XRD pattern of corresponding sample (Figure 1b), the strongest refection is (100), which is quite different from the literature data (JCPDS No. 16-0334). This abnormal intensity of the (100) peak suggests the preferential orientation growth along the [0001] direction to a great degree. At pH = 7, the different crystallographic planes can be recognized on the basis of the similar morphologies and crystal planes,[29] as shown in the top inset of Figure 3D. The presence of the conical ends demonstrates that the crystals grow along the [10$\bar{1}$1] direction to some degree. Moreover, the unchanged size in length further confirms that the growth rate in the [0001] direction is basically maintained, but the size enhancement in diameter demonstrates that the growth velocity in [10$\bar{1}$0] direction is much faster relative to the case of pH = 3 (**S1**). However, in a basic environment (pH = 10), the hexagonal microprisms with very regular hexagonal concave centers on the top/bottom surfaces are produced. The average diameter of these microprisms enhances to 4.5 μm, while the length reduces to 5 μm with respect to **S1**. This indicates that, under the alkaline condition, the dominant adsorption of Cit^{3-} onto the {0001} facets lowers the surface energy of these facets, consequently prohibits the radial enlargement in [0001] direction and drives the growth of nuclei along six symmetric directions of ±[10$\bar{1}$0], ±[1$\bar{1}$00], and ±[01$\bar{1}$0]. In other words, Cit^{3-} has the function of inhibiting significantly the longitudinal growth along the [0001] orientation with a relative enhancement of the growth sideways in the form of 2D hexagonal prisms.

B. pH Values with NaF as Fluoride Source. Under the conditions of NaF as fluoride source and pH = 10 and 11, Cit^{3-} molecules selectively adsorb strongly onto the {0001} surfaces of the growing β-$NaYF_4$ seeds, which prohibits remarkably the [0001] directed growth and promotes the crystal growth mainly along the [10$\bar{1}$0] and [10$\bar{1}$1] directions. The octadecahedral structure obtained at pH = 11 is enclosed by six {10$\bar{1}$0} and twelve {10$\bar{1}$1} facets, as illustrated in Scheme 1b. However, the protruding centers of hexagonal prisms obtained at pH = 10 reveal the tendency to grow along the [10$\bar{1}$1] direction to some degree but not more prominent than octadecahedral structures obtained at pH = 11.

To sum up, when the fluoride source is the same and the pH values are different, the ability of Cit^{3-} to adsorb to certain crystal facets is different from each other, directly leading to the different growth velocity of the different crystal faces, resulting in formation of the anisotropic hexagonal rod or prismatic geometries of the β-$NaYF_4$ crystals.

C. Fluoride Sources under the Same pH Value Condition. Comparing **S1** with **S6** or **S5** with **S8**, with the exception of the use of different fluoride sources NaF and NH_4F, these microstructured β-$NaYF_4$ with different morphologies were synthesized under the identical reaction conditions of $[Y^{3+}] = 0.2$ M, the same pH values, and at 180 °C for 24 h, indicating that the nature of fluoride sources contributes to the formation of various architectures. Concretely speaking, the cations NH_4^+ and Na^+ in the reaction system have a guiding effect on the formation of the change in the microstructures of the as-prepared β-$NaYF_4$ crystals. Wang and co-workers[20a,b] had suggested that the cations coming from the different fluoride sources XF ($X = K^+$, H^+, NH_4^+, Na^+, Rb^+, Cs^+) selectively adsorbed on the different crystals facets of EuF_3 nanoparticle, resulting in the formation of various shapes. Other workers have found that the simple ions direct the growth of nanoparticles into different shapes, highlighting the importance of these species.[9,29] Filankembo and co-workers[30] demonstrated that the control of copper nanocrystal shape can be influenced by the addition of simple RX ($R = Na^+$, K^+; $X = Cl^-$, Br^-, NO_3^-, and HSO_3^-) salts. It is therefore reasonable to assume a similar situation for the effects of the cations Na^+ and NH_4^+ on morphologies. At the early stage of the reactions, due to the strong interactions between Na^+ and NH_4^+ cations and fluoride anions, these two cations can be selectively adsorbed on specific facets of the initial $NaYF_4$ crystals and change their surface energy. However, owing to different sizes of Na^+ and NH_4^+, the relative growth rate of various crystal facets is different from each other, leading to the formation of a variety of morphologies.

In summary, there are two important key factors for determining the final shapes of β-$NaYF_4$ microcrystals. The first one is an intrinsic factor (the crystallographic phase of the nucleated seeds). The $\alpha \rightarrow \beta$ phase conversion leads directly to the morphology variation. The reason is that the anisotropic structures of the thermodynamically stable β-phase $NaYF_4$ seeds induce anisotropic growth along their crystallographically reactive directions; thus, anisotropic shapes of microcrystals are expected. The other one is external factors (pH values and fluoride sources). If the fluoride source and other conditions are the same, fairly dramatic differences of pH values lead directly to the different selective adsorption ability of Cit^{3-} anions on the different crystal facets, consequently resulting in the different shape evolution of β-$NaYF_4$ crystals. On the contrary, if the pH is the same, the fluoride source is different, and other conditions are identical, the cations NH_4^+ and Na^+ in the reaction system have a guiding effect on the morphology variations of the as-prepared microstructured β-$NaYF_4$ crystals. As a result, the different pH values combined with fluoride sources are responsible for the formation of various shapes. We speculate that the influence of fluoride sources and the pH values on the growth of the $NaYF_4$ crystals may lie in four aspects: influencing the interactions between Na^+ and NH_4^+ cations and fluoride anions, affecting the adsorption of Cit^{3-} onto different crystal facets, changing the relative surface energy of the different crystal facets, and affecting the controlling growth mechanism. Scheme 2 shows the possible formation mechanism of the β-$NaYF_4$ microcrystals with different morphologies under different experimental conditions.

(29) (a) Zhou, X. F.; Zhang, D. Y.; Zhu, Y.; Shen, Y. Q.; Guo, X. F.; Ding, W. P.; Chen, Y. *J. Phys. Chem. B* **2006**, *110*, 25734. (b) Hu, J. Q.; Li, Q.; Wong, N. B.; Lee, C. S.; Lee, S. T. *Chem. Mater.* **2002**, *14*, 1216.

(30) Filankembo, A.; Pileni, M. P. *J. Phys. Chem. B* **2000**, *104*, 5865.

Scheme 2. Schematic Illustration of the Possible Formation Processes of the β-$NaYF_4$ Microcrystals with Various Morphologies under Different Experimental Conditions

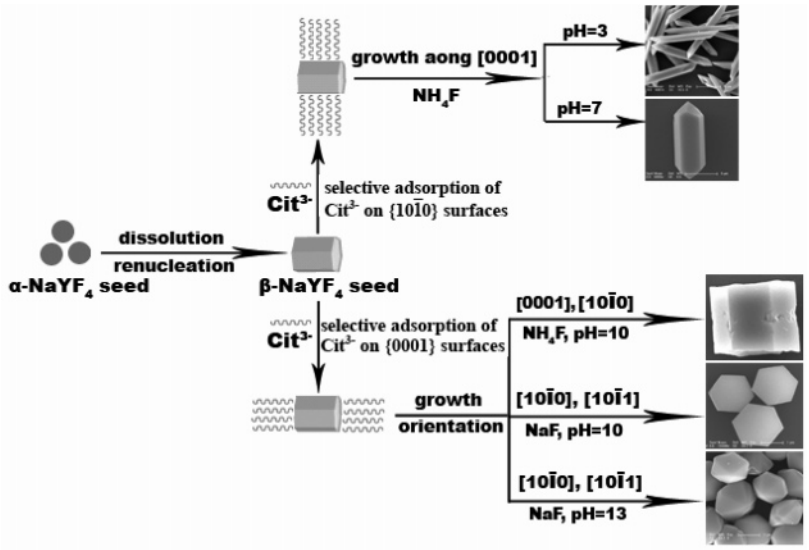

Photoluminescence Properties of Tb^{3+}-Doped β-$NaYF_4$ Microcrystals. β-$NaYF_4$ is regarded as an efficient host lattice for DC and UC process due to the lower phonon energies. Here, we select Tb^{3+} as the doping ion to investigate the spectral and luminescent properties of the products with various morphologies. It is noted that the doping with Tb^{3+} (5 mol %) alters neither the crystal structure nor the morphology of the host material. Figure 9 presents the room-temperature photoluminescence (PL) excitation (a) and emission (b) spectra of the resulting β-$NaYF_4$:5% Tb^{3+} phosphors with microrod (**S1**, black line), hexagonal microprism (**S5**, red line), and octadecahedral (**S7**, green line) shapes, respectively. It can be seen clearly that, in all three samples, the excitation and emission spectra are similar in shape, and the bands differ only in their intensities. The excitation spectrum (Figure 9a) is composed of the characteristic f−f transition lines within the Tb^{3+} $4f^8$ configuration. Basically, the main excitation lines can be assigned as the transitions from the $^7F_6$ ground state to the different excited states of Tb^{3+}, i.e., 288 nm ($^5I_6$), 306 nm ($^5H_6$), 321 nm ($^5D_0$), 344 nm ($^5G_2$), 356 nm ($^5D_2$), 372 nm ($^5G_6$), and 382 nm ($^5D_3$), respectively.[31] Upon excitation into the $^7F_6 \rightarrow {}^5D_2$ transition at 356 nm, the obtained emission spectrum exhibits four obvious lines centered at 488, 544, 584 and 619 nm, originating from the transitions from the $^5D_4$ excited-state to the ^7F_J ($J = 6, 5, 4, 3$) ground states of Tb^{3+} ion, respectively (Figure 9b), with the $^5D_4 \rightarrow {}^7F_5$ transition at 544 nm as the most prominent group. Under identical measurement conditions, the relative intensities of three samples are different, namely, the octadecahedral particles (**S7**) have the highest relative emission intensity, while the prismatic microrod ones (**S1**) show the lowest intensity, and the relative intensity of the former is almost 2 times as high as that of the latter. We ascribe the difference of luminescence relative intensities to the different morphologies and sizes of the three samples. The reasons are as follows. First, although different fluoride sources are used,

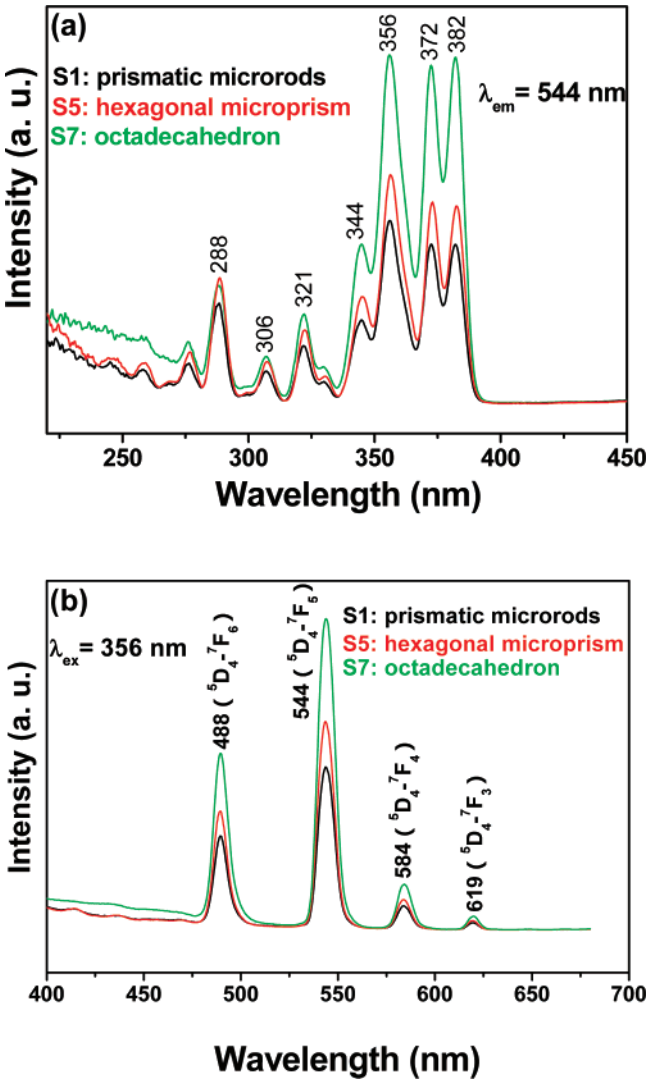

Figure 9. Room-temperature excitation ($\lambda_{em} = 544$ nm) (a) and emission ($\lambda_{ex} = 356$ nm) (b) spectra of 5% Tb^{3+}-doped β-$NaYF_4$ microcrystals with different shapes (as denoted in the inset by different colors).

the crystal phase of the three products is the same, i.e., hexagonal β-$NaYF_4$. Second, the three samples were all

(31) Thomas, K. S.; Singh, S.; Dieke, G. H. *J. Chem. Phys.* **1963**, *38*, 2180.

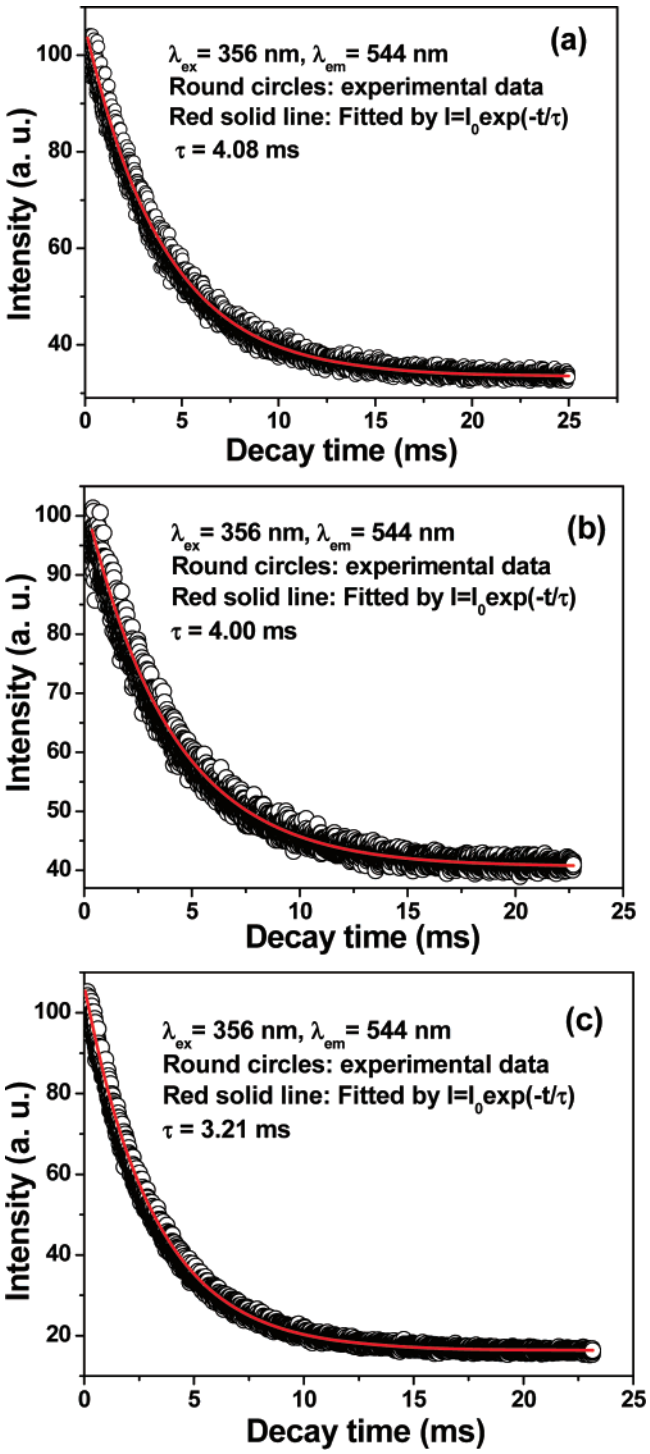

Figure 10. The decay curves for the $^5D_4 \rightarrow {}^7F_5$ emission of Tb^{3+} in β-$NaYF_4$: 5% Tb^{3+} with different morphologies: (a) microrod, (b) microprism, (c) octadehedron. The fitted lifetime values are indicated inside the figures.

treated hydrothermally at 180 °C for 24 h. Third, the precipitates have been washed with deionized water and ethanol in sequence by a centrifugation−redispersion process, so there is no existence of residual NaF and NH_4F in the solid products. On the basis of the above analyses, it is reasonable to believe that the different luminescence properties of the products arise from their morphologies and sizes. In fact, there are several reports concerning the effects of different morphologies and sizes on the emission intensities of the products with the same crystal structures.[20,32] But at this stage, it cannot be fully understood why β-$NaYF_4$:5% Tb^{3+} with octadecahedral morphology shows higher emission intensity than those with other morphologies. It is well-known that the lower the symmetry around the emitting ion, the stronger the emission in lattices.[16,33] It is assumed that the microenvironmental symmetry of Tb^{3+} ions in all samples are similar. However, after excitation, octadecahedronal **S7** has 18 faces for the emitting light to come out, while the hexagonal microprism (**S5**) (or microrod **S1**) has only eight (or less) faces for the light to come out. This might lead the relative emission intensity of **S7** to be higher than that of **S5** and **S1**. Simultaneously, the PL decay curves (Figure 10) for the luminescence of Tb^{3+} in **S1**, **S5**, and **S7** can further substantiate the above result. These curves can be well-fitted by a single-exponential function as $I(t) = I_0 \exp(-t/\tau)$ (I_0 is the initial emission intensity at $t = 0$ and τ is the 1/e lifetime of the emission center), and the lifetimes for $^5D_4$ (detected at 544 nm for $^5D_4 \rightarrow {}^7F_5$ transition) of Tb^{3+} were determined to be 4.08 ms (**S1**, microrod shape), 4.00 ms (**S5**, microprism shape), and 3.21 ms (**S7**, octadehedral shape), as shown in parts a, b, and c in Figure 10, respectively. Because there is no quenching group such as the hydroxyl group in three samples, the simple decay curves indicate that the observed emission is a simple radiative processes and no other nonradiative process occur in the $^5D_4$ state in three samples. According to the literature,[34] the shorter the emission lifetime, the stronger the emission intensities. So it is reasonable that the octadehedrally shaped **S7** with shortest lifetime possesses the strongest emission intensity. These observations show that the size and shape are strongly related to the luminescence properties of a material, which is deserving of investigation in other systems.

4. Conclusions

In summary, systematic manipulation of the morphologies and architectures of β-$NaYF_4$ microcrystals on a large scale has been successfully achieved using a simple and mild solution-growth method free of any templates and catalysts. The influences of fluoride sources and pH value on the shapes of β-$NaYF_4$ microstructures have been investigated in detail. The intrinsic hexagonal structure of β-$NaYF_4$ and a variety of external factors account for the ultimate shape evolutions of the products. It is meaningful to investigate the morphological growth process of β-$NaYF_4$ microcrystals, which can provide important information to the fields of crystal growth and design and may be extended to morphology-controlled creation of other rare earth fluoride systems with complex forms. In addition, the experimental results indicate that the optical properties of the β-$NaYF_4$:Tb^{3+} phosphors with different microarchitectures are strongly dependent on their morphologies and sizes.

(32) (a) Kim, F.; Connor, S.; Song, H.; Kuykendall, T.; Yang, P. D. *Angew. Chem., Int. Ed.* **2004**, *43*, 3673. (b) Geng, J.; Zhu, J. J.; Chen, H. Y. *Cryst. Growth Des.* **2006**, *6*, 321. (c) Zhou, H. J.; Mao, Y. B.; Wong, S. S. *J. Mater. Chem.* **2007**, *17*, 1707.
(33) Zakaria, D.; Mahiou, R.; Avignant, D.; Zahir, M. *J. Alloy Compd.* **1997**, *257*, 65.
(34) Chiang, P. Y.; Lin, T.-W.; Dai, J.-H.; Chang, B.-C.; Lii, K.-H. *Inorg. Chem.* **2007**, *46*, 3619.

Acknowledgment. This project is financially supported by the foundation of "Bairen Jihua" of Chinese Academy of Science, the MOST of China (2003CB314707, 2007CB935502), and the National Natural Science Foundation of China (NSFC 50572103, 20431030 and 00610227).
CM071668G